

# Mode I fracture of adhesive joints using tailored cohesive zone models

M. Alfano · F. Furgiuele · A. Leonardi ·  
C. Maletta · G. H. Paulino

Received: 16 June 2008 / Accepted: 24 November 2008 / Published online: 16 December 2008  
© Springer Science+Business Media B.V. 2008

**Abstract** Cohesive zone models are explored in order to study cleavage fracture in adhesive bonded joints. A mode I cohesive model is defined which correlates the tensile traction and the displacement jump (crack faces opening) along the fracture process zone. In order to determine the traction-separation relation, the main fracture parameters, namely the cohesive strength and the fracture energy, as well as its shape, must be specified. However, owing to the difficulties associated to the direct measurement of the fracture parameters, very often they are obtained by comparing a measured fracture property with numerical predictions based on an idealized traction separation relation. Likewise in this paper the cohesive strength of an adhesive layer sandwiched between elastic substrates is adjusted to achieve a match between simulations and experiments. To this aim, the fracture energy and the load-displacement curve are adopted as input in the simulations. In order to assess whether or not the shape of the cohesive model may have an influence on the results, three representative cohesive zone models

have been investigated, i.e. exponential, bilinear and trapezoidal. A good agreement between experiments and simulations has been generally observed. However, a slight difference in predicting the loads for damage onset has been found using the different cohesive models.

**Keywords** Adhesives · Cohesive zone model · Cohesive zone model shape · Fracture energy

## 1 Introduction

Adhesive bonding is recognized as a potential alternative to the traditional fastening methods in many industrial applications (e.g. automotive, aerospace, constructions, microelectronics, etc). In order for joints to exhibit high toughness and fatigue strength, accurate substrate surface preparation is required (Kinloch 1986). Nevertheless, actual joints are often flawed, and inaccurate fabrication or curing may cause the presence of bubbles, dust particles or un-bonded areas along the bondline. The extension of these pre-existing flaws induces complex damage mechanisms and multiple failure modes (Akisanya and Fleck 1992). As the direct inspection of the joints is generally not feasible, non-destructive testing methods are the usual choice for integrity assessment purposes (Goglio and Rossetto 2002). However, damage detection in adhesive joints remains a difficult task and therefore engineering structures are often designed to be tolerant to reasonably-sized flaws.

---

M. Alfano (✉) · F. Furgiuele · A. Leonardi · C. Maletta  
Department of Mechanical Engineering, University  
of Calabria, Via Ponte P. Bucci, Cubo 44C,  
87036 Arcavacata di Rende, Italy  
e-mail: alfano@unical.it

G. H. Paulino  
Department of Civil and Environmental Engineering,  
University of Illinois at Urbana-Champaign, Newmark  
Laboratory, 205 N. Mathews Avenue, Urbana,  
IL 61801-2352, USA

Linear Elastic Fracture Mechanics (LEFM) has proven to be a useful tool and allowed for a more rapid extension of adhesives technology into engineering applications. The major advantage of LEFM is its simplicity. So far the single parameter treatment based on the stress intensity factor (or, equivalently, on the energy release rate) has been extensively and successfully applied to tackle fracture events in adhesive joints—see for instance Mostovoy and Ripling (1971); Blackman et al. (1991, 2003a, b). However, LEFM can only be used with the assumed presence of an initial crack (or crack-like defect) concurrent with a relatively small size of the non-linear zone at crack tip compared to the overall dimensions of the specimens.

A valid alternative to LEFM for those problems in which these conditions may not be met consists of using a Cohesive Zone Model (CZM) approach (e.g. Dugdale 1960, Barenblatt 1962). In this approach, the entire fracture process is lumped into the crack line and is characterized by a cohesive model which relates tractions ( $T$ ) and displacement jumps ( $\Delta$ ) across cohesive surfaces. With increasing separation the traction increases, reaches a maximum (cohesive strength) and then, governed by the softening curve, decreases and eventually vanishes allowing for traction-free crack surface creation.

Although the overall CZM approach dates back to the theoretical studies of early 1960s, the concept has gained widespread use in recent time with its numerical implementation, especially in the Finite Element (FE) framework (Xu and Needleman 1994; Zhang 2007). To date, CZM has been successfully applied to model fracture for a wide class of materials, e.g. metals, concrete, polymers, ceramics, composites (Zavattieri and Espinosa 2001; Zhang and Paulino 2005; Scheider and Brocks 2006; Song et al. 2006a, b; Roesler et al. 2007a, b; Park et al. 2008) and its range of applications continue to expand.

An important issue related to the use of CZM is the determination of the traction-separation relation. In particular, the relevant fracture parameters, such as fracture strength and fracture energy, as well as the shape of the traction-separation relation, must be specified. Owing to the difficulties associated to the direct measurement of the these parameters, very often they are obtained simply by comparing a measured fracture property with numerical predictions based on an idealized cohesive model—see for instance (Cox and Marshall 1991; Blackman et al. 2003c; Liljedhal et al. 2006;

Song et al. 2006a, b). Cohesive strength and fracture energy are believed to have greater importance with respect to the specific shape chosen for the cohesive model (Kafkalidis et al. 2000). Therefore, many traction-separation relations have been employed in the literature, e.g. the potential based exponential model (Xu and Needleman 1994), the trapezoidal model (e.g. Tvergaard and Hutchinson 1996) and the bilinear model (e.g. Zhang and Paulino 2005; Liljedhal et al. 2006) are perhaps the most widely adopted.

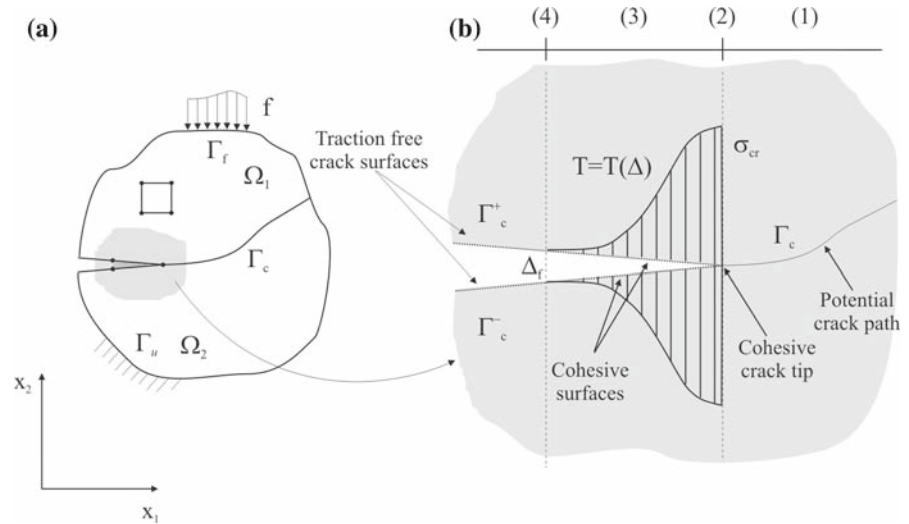
In this paper, CZM concepts are applied to study fracture in adhesive joints. To this aim, a proper Cohesive Zone Element (CZE) is implemented in a FE commercial code (ABAQUS 2002). The CZE implemented is tested using experimental data supplemented by the literature (Pirondi and Nicoletto 2000). In particular, the sensitivity of cohesive zone parameters in predicting the mechanical response of the specimen is examined. In addition, as the shape of the actual cohesive zone model may affect the numerical simulations (Williams and Hadavinia 2002; Sorensen and Jacobsen 2003; Shet and Chandra 2004; Volokh 2004; Alfano 2006a; Song et al. 2008), the results obtained using widely adopted traction-separation relations (i.e. trapezoidal, bilinear and exponential model) are compared. Afterwards, the CZEs developed are used to study crack propagation behavior in the Double Cantilever Beam (DCB) specimens prepared using aluminium (AA6060-TA16) substrates and two component epoxy resin (Loctite Hysol 9466, Henkel, Germany).

## 2 Basic cohesive zone model (CZM) concepts

Let's consider the domain  $\Omega$  as shown in Fig. 1a. The material discontinuity,  $\Gamma_c$ , defines an interface between the sub-domains  $\Omega_1$  and  $\Omega_2$  and represents an internal surface, namely a cohesive surface, not yet separated. Prescribed tractions,  $f_i$ , are imposed on the surface boundary  $\Gamma_f$ . If the body forces are neglected, the stress field,  $\sigma_{ij}$ , can thus be related to the external loading and to the closing tractions,  $T_i$ , in the material discontinuity through the following relations:

$$\begin{cases} \frac{\partial \sigma_{ij}}{\partial x_j} = 0 & \text{in } \Omega = \Omega_1 \cup \Omega_2, \\ \sigma_{ij} n_j = f_i & \text{on } \Gamma_f, \\ u_i = \bar{u}_i & \text{on } \Gamma_u, \\ \sigma_{ij} n_j = T_i & \text{on } \Gamma_c, \end{cases} \quad (1a-d)$$

**Fig. 1** Cohesive Zone Model concept



where  $n_j$  is the outward normal, and  $\bar{u}_i$  are the prescribed displacements on the boundary  $\Gamma_u$ .

In the simplest formulation of CZM, the whole body volume remains elastic while the nonlinearity is embedded in the cohesive model, which dictates the boundary conditions along the crack line,  $\Gamma_c$  (Fig. 1b). The peak stress on the traction-separation relation is considered to be the cohesive strength,  $\sigma_{cr}$ , of the material, while the area under the curve is associated to the cohesive fracture energy.

It is worth noting that the fracture energy for an adhesive layer involves the intrinsic fracture energy ( $G_o$ ) required for breaking the intrinsic bonding forces and a visco-elastic and/or plastic energy terms ( $\psi$ ) which accounts for energy dissipation in the surrounding adhesive layer (Kinloch 1986). The latter usually represents the main sources of energy absorption in a ductile adhesive. Therefore the adhesive fracture energy is usually written as

$$G_c = G_o + \psi. \tag{2}$$

Similarly to the work by Yang et al. (1999) and Ferracin et al. (2003), the entire adhesive layer will be replaced by a single row of cohesive elements. Because the macroscopic response of the adhesive layer is represented by the cohesive zone, the failure process in the adhesive ( $G_o$ ) and the elasto-plastic deformation in the bulk of the adhesive ( $\psi$ ) are directly embodied in the traction-separation relation. The layer can be also modeled as an elastoplastic continuum with fracture parameters (Yuan and Xu 2008; Pardoen et al. 2005; Martiny et al.

2008), but this procedure is not adopted in the present work.

The CZM fracture process can be summarized as illustrated in Fig. 1b: at first a linear elastic material response prevails (1), as the load increases the crack initiates (2), and then it evolves from initiation to complete failure (3) with the appearance of new traction free crack surfaces,  $\Gamma_c^-$  and  $\Gamma_c^+$  ( $\Delta = \Delta_f$ ) (4). Therefore, material constitutive behavior is split in two parts: a linear stress-strain relation for the bulk material and a cohesive surface relation, which allows for crack initiation and growth, for the cohesive surfaces. From this standpoint, many cohesive zone models have been proposed in the literature: the potential-based exponential model and the (non-potential based) trapezoidal and bilinear models are widespread to model fracture in adhesive joints (Tvergaard and Hutchinson 1996; Ferracin et al. 2003; Blackman et al. 2003b,c; Xu et al. 2003; Pardoen et al. 2005; Martiny et al. 2008). In this paper these traction-separation relations have been implemented in order to investigate fracture behavior of adhesive joints (Fig. 2).

The development of cohesive zone models in the FE framework thus requires bulk finite elements bordered by cohesive surface elements with embedded cohesive surface relations. From this point of view there are basically two approaches which differ in the way by which cohesive surface elements are inserted in the initial geometry. In the *intrinsic* approach (Xu and Needleman 1994) cohesive elements are introduced between volumetric elements from the beginning of the analysis

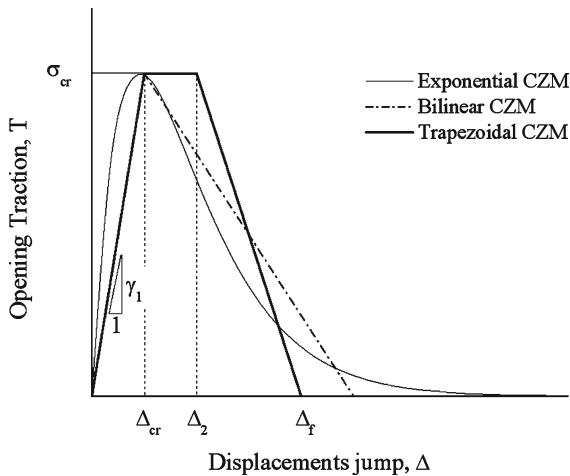


**Fig. 2** Schematic representation of the cohesive models examined in the paper

as a network of cohesive surfaces. With increasing separation, cohesive traction increases from zero, reaches the cohesive strength and then decreases (e.g. back to zero or to a small value) following the post peak softening behavior. This network of cohesive surfaces introduces artificial compliance due to the finite initial stiffness of the cohesive model. In the *extrinsic* approach (Camacho and Ortiz 1996; Zhang and Paulino 2005), cohesive elements are introduced adaptively in the mesh according to a proper activation criterion: thus the adopted model is a rigid one with softening. In the present paper, the fracture behavior of adhesive joints is analyzed using intrinsic cohesive zone models. The particular problem of adhesive joints requires cohesive surface elements introduced along a predefined fracture path, i.e. the bond line. Thus the number of cohesive interface is significantly reduced and this, in turn, yields a low or negligible compliance. The traction-separation relations analyzed in this paper are now briefly summarized.

### 2.1 Exponential model (potential-based)

The cohesive traction according to the exponential model is derived through a cohesive potential energy  $\phi$  and is given as follows (Xu and Needleman 1994)

$$T = \frac{\partial \phi}{\partial \Delta} = \left( \frac{\Delta}{\Delta_{cr}} \right) \sigma_{cr} \exp \left( 1 - \frac{\Delta}{\Delta_{cr}} \right), \quad (3)$$

where the notation is consistent with the definitions previously given (cf. Fig. 2). As crack face displacements

increase, the traction increases, reaches a maximum, and then decays monotonically. The traction integrated to complete separation yields the cohesive fracture energy

$$G_c = \sigma_{cr} \Delta_{cr} \exp(1). \quad (4)$$

### 2.2 Bilinear model

The analytical expression of the bilinear model is given as follows (Zhang and Paulino 2005; Liljedhal et al. 2006)

$$T = \begin{cases} \gamma_1 \Delta & \Delta \leq \Delta_{cr} = \gamma_1 \Delta_f, \\ \sigma_{cr}(\Delta_f - \Delta) / (\Delta_f - \Delta_{cr}) & \Delta_{cr} < \Delta \leq \Delta_f, \\ 0 & \Delta > \Delta_f, \end{cases} \quad (5)$$

where  $\gamma_1$  is the initial stiffness of the cohesive zone model and  $\Delta_f$  is the crack face opening at which material separation occurs (cf. Fig. 2). The normal work of separation is then given by

$$G_c = \sigma_{cr} \Delta_f / 2. \quad (6)$$

### 2.3 Trapezoidal model

The analytical expression of the trapezoidal traction-separation model (Tvergaard and Hutchinson 1996) is given as follows

$$T = \begin{cases} \gamma_1 \Delta & \Delta \leq \Delta_{cr} = \gamma_1 \Delta_f, \\ \sigma_{cr} & \Delta_{cr} < \Delta \leq \Delta_2 = \lambda_2 \Delta_f, \\ \sigma_{cr}(\Delta_f - \Delta) / (\Delta_f - \Delta_2) & \Delta_2 < \Delta \leq \Delta_f, \\ 0 & \Delta > \Delta_f. \end{cases} \quad (7)$$

Accordingly, the normal work of separation is given by

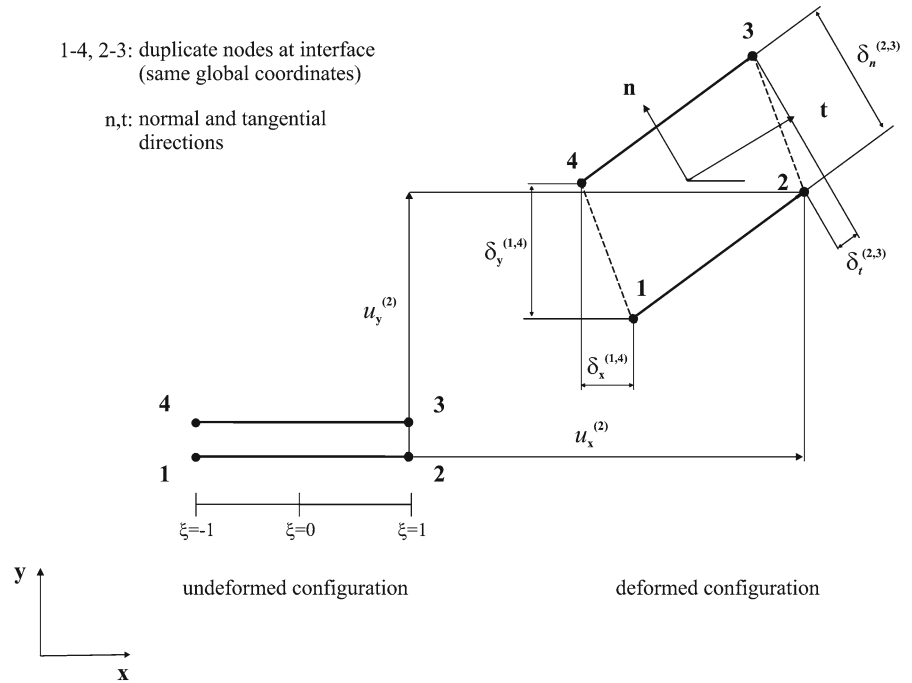
$$G_c = \sigma_{cr} \Delta_f (1 + \lambda_2 - \gamma_1) / 2. \quad (8)$$

As it can be seen, for this particular (T- $\Delta$ ) curve, the governing cohesive parameters are the cohesive fracture energy ( $G_c$ ), the peak stress ( $\sigma_{cr}$ ), and the critical opening displacement ( $\Delta_f$ ) while  $\gamma_1$  and  $\lambda_2$  dictate the shape of the  $T = T(\Delta)$  relation (cf Fig. 2).

### 2.4 Implementation in the FE framework

In this paper, four node cohesive zone elements (CZE) with two integration points have been implemented

**Fig. 3** Four-noded cohesive zone element



within the commercial FE code ABAQUS using the user element (UEL) capability (Alfano 2006b). A schematic representation of a CZE is given in Fig. 3.

A CZE is made up of two linear line elements (cohesive surfaces) that connect the faces of adjacent elements during the fracture process. The two surfaces initially lie together in the unstressed deformation state (zero thickness) and, subsequently, separate as the adjacent elements deform following the corresponding traction-separation model. In order to carry out the iterations of the method, the contributions of cohesive elements to the tangent stiffness matrix as well as to the force vector are acquired. The implementation of a general cohesive element is briefly explained below. The line cohesive element has eight degrees of freedom. In particular, the nodal displacements vector in the global coordinate system is given as

$$\mathbf{u}_g = \left\{ u_x^{(1)} \ u_y^{(1)} \ u_x^{(2)} \ u_y^{(2)} \ u_x^{(3)} \ u_y^{(3)} \ u_x^{(4)} \ u_y^{(4)} \right\}^T, \quad (9)$$

in which the order follows typical convention. Crack-faces opening for cohesive elements is defined as the difference between top and bottom nodes thereby leading to the following definition in terms of displacements of paired nodes

$$\begin{aligned} \begin{Bmatrix} \delta_x^{(1,4)} \\ \delta_y^{(1,4)} \\ \delta_x^{(2,3)} \\ \delta_y^{(2,3)} \end{Bmatrix} &= \begin{Bmatrix} u_x^{(1)} - u_x^{(4)} \\ u_y^{(1)} - u_y^{(4)} \\ u_x^{(2)} - u_x^{(3)} \\ u_y^{(2)} - u_y^{(3)} \end{Bmatrix} = \mathbf{L} \mathbf{u}_g \\ &= \begin{bmatrix} 1 & 0 & 0 & 0 & 0 & 0 & -1 & 0 \\ 0 & 1 & 0 & 0 & 0 & 0 & 0 & -1 \\ 0 & 0 & 1 & 0 & -1 & 0 & 0 & 0 \\ 0 & 0 & 0 & 1 & 0 & -1 & 0 & 0 \end{bmatrix} \mathbf{u}_g, \end{aligned} \quad (10)$$

with  $\mathbf{L}$  being an operator localization matrix. From the nodal positions, the crack face opening is interpolated to the Gauss integration points by means of standard shape functions

$$\tilde{\Delta} = \begin{Bmatrix} \delta_x \\ \delta_y \end{Bmatrix} = \begin{bmatrix} \frac{1-\xi}{2} & 0 & \frac{1+\xi}{2} & 0 \\ 0 & \frac{1-\xi}{2} & 0 & \frac{1+\xi}{2} \end{bmatrix} \begin{Bmatrix} \delta_x^{(1,4)} \\ \delta_y^{(1,4)} \\ \delta_x^{(2,3)} \\ \delta_y^{(2,3)} \end{Bmatrix} = \mathbf{N} \mathbf{L} \mathbf{u}_g, \quad (11)$$

where  $\xi$  is the natural coordinate and  $\mathbf{N}$  is the matrix of shape functions. Because the constitutive relations are based on tractions and displacements in the local coordinate system, a transformation from global to local coordinate is needed for the cohesive element. Let  $\mathbf{R}$  define the orthogonal transformation matrix from global

(x, y) reference frame to element specific local coordinate system. Then the relative displacement vector, for an uncoupled cohesive model, is given as

$$\mathbf{\Delta} = \mathbf{R}\tilde{\mathbf{\Delta}} = \mathbf{R}\mathbf{N}\mathbf{L}\mathbf{u}_g = \mathbf{B}\mathbf{u}_g. \tag{12}$$

The relative displacements of the element faces create normal and shear displacements, which in turn generate element stresses depending on the constitutive equations of the material. The relationship between tractions and displacements is given by

$$\mathbf{T} = \frac{\partial \mathbf{T}}{\partial \mathbf{\Delta}} \mathbf{\Delta}, \tag{13}$$

where

$$\frac{\partial \mathbf{T}}{\partial \mathbf{\Delta}} = \begin{bmatrix} \frac{\partial T_t}{\partial \Delta_t} & 0 \\ 0 & \frac{\partial T_n}{\partial \Delta_n} \end{bmatrix}, \tag{14}$$

is the Jacobian stiffness matrix while the subscripts *t* and *n* denote the tangential and normal directions (cf. Fig. 3). The constitutive relationships adopted herein have been presented in the previous section and they are independent of the element formulation. The stiffness matrix for cohesive elements can be obtained by minimizing the total amount of potential energy

$$\Pi = U + W = \frac{1}{2} \int_A \mathbf{\Delta}^T \mathbf{T} dA - \mathbf{u}_g^T \mathbf{f}, \tag{15}$$

where

$$\left[ \int_A \mathbf{B}^T \frac{\partial \mathbf{T}}{\partial \mathbf{\Delta}} \mathbf{B} dA \right] \mathbf{u}_g = \mathbf{f}, \tag{16}$$

in which **f** is the external traction vector; after some manipulation, it follows that the cohesive element stiffness matrix is given as

$$\mathbf{K} = \int_A \mathbf{B}^T \frac{\partial \mathbf{T}}{\partial \mathbf{\Delta}} \mathbf{B} dA = \int_{\Gamma} \mathbf{B}^T \frac{\partial \mathbf{T}}{\partial \mathbf{\Delta}} \mathbf{B} w d\Gamma, \tag{17}$$

where *w* is the element width. The contribution of cohesive elements to the global force vector is defined, in a variational setting, using the principle of virtual work

$$\delta \Pi_{INT} = \delta \Pi_{EXT} \Leftrightarrow \int_A \delta \mathbf{\Delta}^T \mathbf{T} dA = \delta \mathbf{u}_g^T \mathbf{F}_{Coh}, \tag{18}$$

with  $\delta \Pi_{INT}$  and  $\delta \Pi_{EXT}$  being the internal and external virtual work respectively. The equivalent right hand side nodal force vector for cohesive elements, **F**<sub>Coh</sub>, is then given as follows

$$\mathbf{F}_{Coh} = \int_A \mathbf{B}^T \mathbf{T} dA = w \int_{\Gamma_c} \mathbf{B}^T \mathbf{T} d\Gamma_c. \tag{19}$$

All analyses have been done using quasi-static, incremental/iterative procedures.

### 3 Model testing with experimental data supplemented by the literature

Initially, the performance of the CZMs developed herein have been assessed using experimental data retrieved from the literature (Pirondi and Nicoletto 2000). As it can be seen in Fig. 4a, the specimen analyzed is a Double Cantilever Beam (DCB) with length (L) equal to 120 mm, substrate thickness (h) of 15 mm, and width (B) of 30 mm. The mechanical pre-notch (*a*<sub>0</sub>) extends 40 mm from the left to the right edge of the beam. Aluminum substrates (*E*<sub>s</sub> = 70 GPa and *v*<sub>s</sub> = 0.33) are bonded with methacrylate adhesive (*E*<sub>a</sub> = 880 MPa and *v*<sub>a</sub> = 0.15). The bond line thickness (*h*<sub>a</sub>) is equal to 0.3 mm. External loading is imposed under displacement control. The measured fracture toughness is *G*<sub>c</sub> = 550 N/m. Plane strain four nodes continuum elements (CPE4) were used for the substrate material.

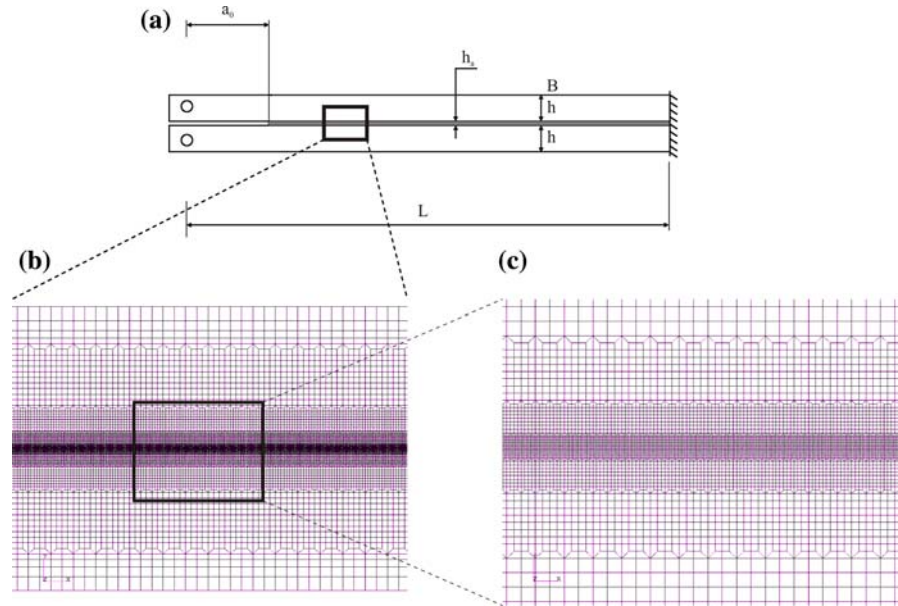
#### 3.1 Modeling approach

In the numerical analysis, the adhesive layer is replaced by a layer of user-defined cohesive elements (Yang et al. 1999; Ferracin et al. 2003; Pardoen et al. 2005). Therefore, the intrinsic work of fracture as well as the inelastic deformation in the bulk adhesive is directly embodied in the traction-separation relation. Cohesive element size has been properly chosen to avoid mesh size dependence. Indeed, the implementation of the CZM concept in the FEM poses the issue related to the sensitivity of cohesive element size to the numerical solutions (Song et al. 2006a, b). With coarser mesh, the shape of the interface model may have a non-negligible influence on the simulated load-displacement curve. This problem can be tackled by means of suitable mesh refinements; usually three or more elements should be inserted in the non linear zone in order to properly represent tractions. In this paper, a cohesive zone element size of 0.08 mm has been chosen based on global energy arguments as reported in (Song et al. 2006a, b; Alfano et al. 2007). Figs. 4b and c show mesh details for the regions where cohesive elements are inserted.

#### 3.2 Sensitivity analysis and calibration of cohesive fracture parameters

A sensitivity analysis to cohesive fracture parameters has been performed. The influence of the simulated

**Fig. 4** **a** Schematic representation of the specimen, **b** and **c** mesh details in the near crack tip zone (minimum element size 0.08 mm)



mechanical responses to cohesive parameters, i.e. material strength ( $\sigma_{cr}$ ) and cohesive fracture energy ( $G_c$ ) has been assessed. Figures 5 and 6 illustrate the sensitivity of  $P$  versus  $\delta$  curve to different fracture energies and cohesive strengths for all the cohesive models examined in the paper. Fig. 5 shows that, when the cohesive strength is held constant, as the fracture energy increases the area under the curve (global fracture energy) and the peak load increases.

On the other hand, when the cohesive fracture energy is held fixed (cf. Fig. 6), as the critical strength increases, the peak load is increased while the global fracture energy is almost constant.

An important issue related to the use of CZM is the determination of the fracture parameters, i.e. fracture strength and fracture energy. In this paper, the cohesive strength has been iteratively adjusted until a match between simulations and experiments was achieved. In particular, the fracture energy and the load-displacement curve reported in (Pirondi and Nicoletto 2000) have been adopted as inputs. The simulated load displacement curves along with the corresponding cohesive parameters that give minimum deviations between simulations and experiments are reported in Fig. 7.

In the elastic range, the response provided by the exponential model is affected by the compliance inherent in this cohesive model. Indeed, the initial slope

of the corresponding load-displacement curve is lower than the others. When bilinear and trapezoidal models are used this effect is reduced. It is worth noting that the cohesive strength adopted for the exponential model is higher than that of the bilinear one; this is a drawback of the exponential model that does not allow control of the initial stiffness without affecting the cohesive strength. On the contrary, in the bilinear CZM, the initial stiffness can be adjusted ensuring a relatively stiff connection between cohesive and bulk elements. Thus, a proper representation of the undamaged state is ensured without affecting the cohesive strength. The lowest value of the cohesive strength, among those that allow to obtain the best fit with experiments, is that obtained for the trapezoidal model. The differences with respect exponential and bilinear models are  $\cong -25\%$  and  $\cong -14\%$ , respectively. Owing to this difference between the estimate values of the cohesive strength, further analysis has been done keeping the fracture parameters constant and equal to  $G_c = 550 \text{ J/m}^2$  and  $\sigma_{cr} = 5 \text{ MPa}$ . The load-displacement curves predicted using similar fracture parameters are compared in Fig. 8.

A good agreement is observed in the elastic range and in the post-peak regions (damage propagation) of the  $P$ - $\delta$  curves. Actually, the bilinear and the exponential models give rise to nearly superimposed responses, but a higher load for damage onset is predicted by the

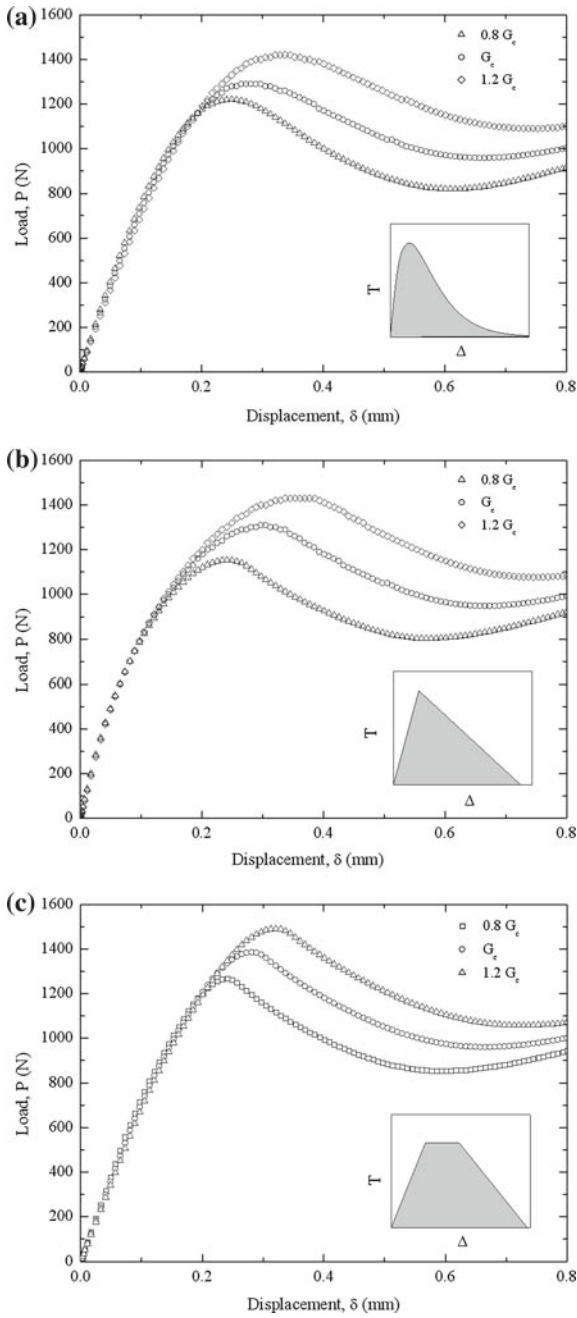


**Fig. 5** Sensitivity of  $P$  versus  $\delta$  curves to cohesive fracture energy: **a** exponential, **b** bilinear and **c** trapezoidal model

trapezoidal model which, therefore, slightly overestimates the peak load. This effect can be addressed to the different interfacial stress profile which it produces with respect to the other ones. However, this differ-

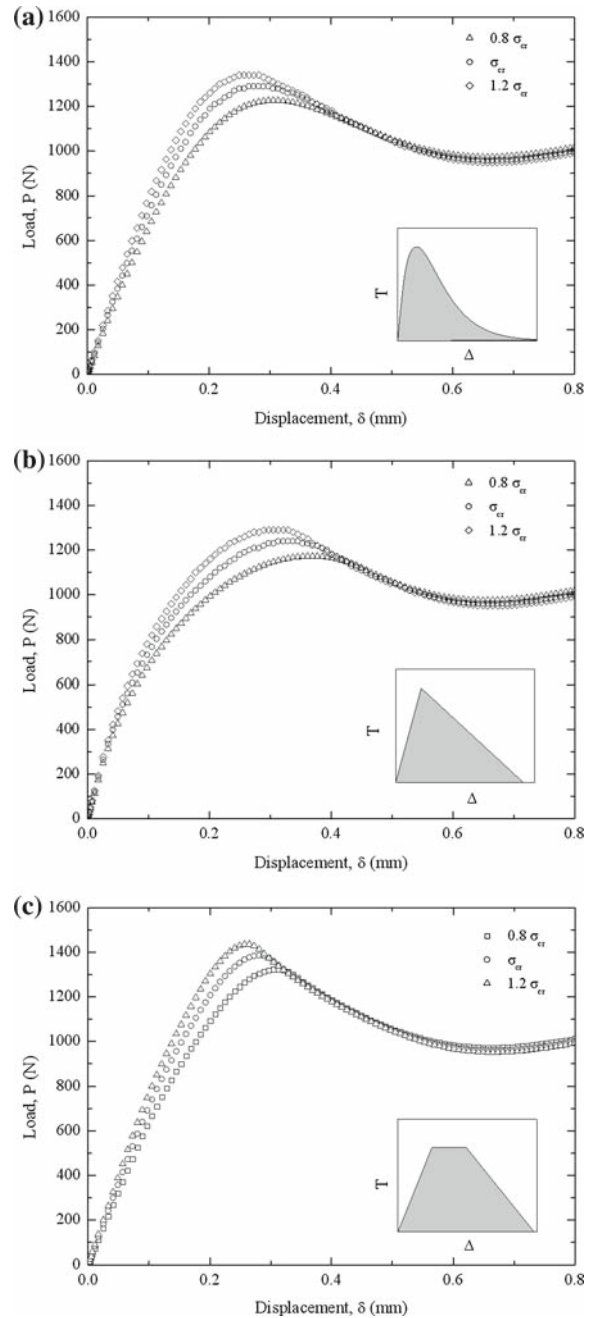


**Fig. 6** Sensitivity of  $P$  versus  $\delta$  curves to cohesive strength: **a** exponential, **b** bilinear and **c** trapezoidal model.

ence in the responses was expected; indeed a lower value of the cohesive strength has been selected for the trapezoidal model in order to match the experimental results.

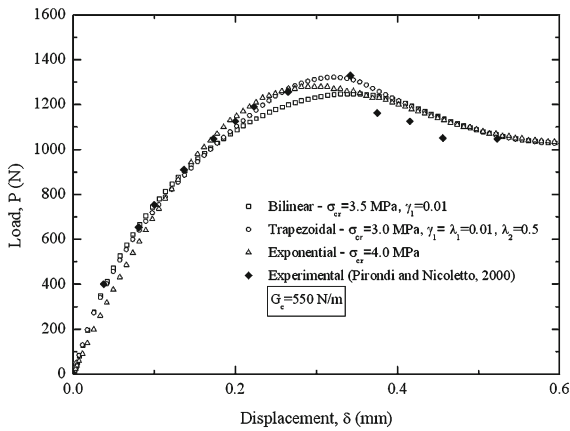


**Fig. 7** Comparison of  $P$  versus  $\delta$  curves between numerical (calibrated) and experimental results

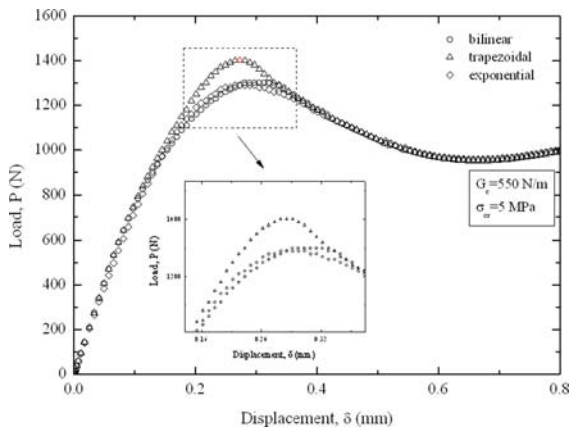


**Fig. 8** Comparison among numerical  $P$  versus  $\delta$  curves obtained keeping cohesive parameters as constants

#### 4 Simulation of fracture in aluminium/epoxy joints

The cohesive zone models previously developed have been then used in conjunction with experimental data generated by the authors. The specimens analyzed herein consist of aluminum (AA6060-TA16) substrates bonded with a two component, medium viscosity and fast curing industrial grade epoxy adhesive (Loctite, Hysol® 9466 A&B) supplied by Henkel (Germany). The substrates have length  $L = 200$  mm, width  $B = 25$  mm and thickness  $t = 15$  mm. Substrate materials were stored in normal (ambient) conditions prior to joint manufacturing. Each material is assumed to be isotropic and linear elastic. In particular, the elastic properties of the aluminum substrates are  $E = 65.7$  GPa

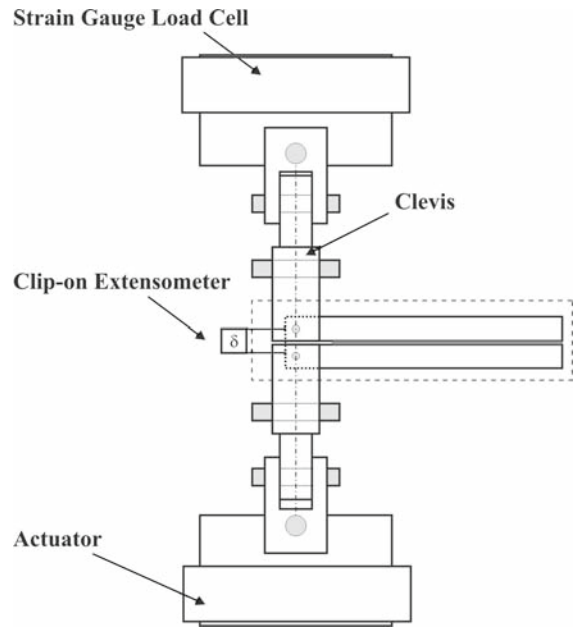


**Fig. 9** Schematic representation of the experimental set-up

and  $\nu = 0.33$ , while those of the epoxy resin provided by the manufacturer are  $E = 1.7$  GPa and  $\nu = 0.35$ .

Substrates surfaces were grit blasted (alumina 80 grit) prior bonding and then cleaned with acetone. The adhesive was applied to each substrate and a bond line thickness equal to 0.6 mm was obtained by placing metallic wires as spacers at each joint end. An initial pre-crack was introduced using a release agent. Specimens were then cured at room temperature ( $25^\circ\text{C}$ ) for about 24 h, so that we can exclude occurrence of any significant residual stresses. Tests were performed at room temperature using a universal testing machine (Instron 8500 plus). Specimens were pin-loaded and tested under displacement control at a constant cross-head feed rate of 0.06 mm/min. To this aim, 6 mm loading holes have been drilled through the substrate. The surfaces of the loading pins were lubricated to reduce frictional effects. In addition, upper and lower loading frames were allowed to pivot about the centerline. In such way, a cleavage opening is ensured and tearing or opening displacement on the joints are thus avoided. The crack mouth opening displacement ( $\delta$ ) was measured using a clip-on extensometer (Instron, 2630 series). A schematic illustration of the experimental set-up is given in Fig. 9.

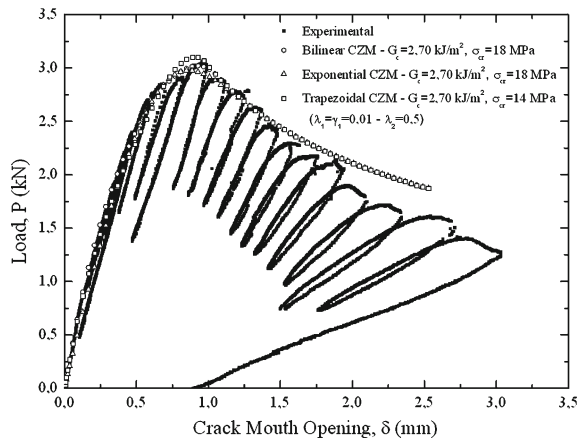


**Fig. 10** Comparison of  $P$  versus  $\delta$  curves between numerical and experimental results for the Al/Epoxy (Al6061T6/Loctite Hysol 9466) material system

The mode I fracture energy of the joint is approximately equal to  $2800 \text{ J/m}^2$  (ASTM D3433). A finite element model of the test specimen has been developed (plane strain four nodes continuum elements were used for the substrate material, and cohesive surface elements were used for replacing the adhesive layer). The fracture energy of the joint was experimentally measured while the cohesive strength was determined by a trial and error procedure until a match between simulations and experiments was achieved. The simulated load displacement curves along with the corresponding cohesive parameters, which give minimum deviations between simulations and experiments, are reported in Fig. 10.

Good agreement between numerical and experimental results is generally observed. The cohesive strength which gives the minimum deviation between experiments and simulations for the bilinear and the exponential model is equal to 18 MPa, whereas for the trapezoidal model it is lower and equal to 14 MPa. This feature, as previously shown, can be addressed to the different interfacial stress profile produced with respect to other models. Moreover, the best fitting was achieved using a fracture energy equal to  $G_c = 2700 \text{ J/m}^2$ , that is nearly equal to measured values reported in the previous section.

## 5 Summary and concluding remarks

In this paper, CZM concepts have been applied in order to study mode I fracture in pre-cracked bonded Double

Cantilever Beam (DCB) specimens. A cohesive surface element has been implemented in a finite element commercial code using intrinsic cohesive zone models: exponential, bilinear and trapezoidal models. In the actual computational practice of CZM, the cohesive fracture parameters are often obtained iteratively comparing a measured property, e.g. a crack opening profile, with the response of a corresponding FE model. The cohesive strength is tuned until the numerical results match the experimental records. Using such procedure, good agreement among various experiments and simulations has been observed using different cohesive zone models. Furthermore, both the bilinear and trapezoidal cohesive zone models are appropriate for modeling the undamaged state of cracked adhesive joints: they can control the pre-peak slope of the traction-separation model allowing to reduce compliance. However, for the system examined herein, the trapezoidal model overestimates the load for damage onset. Indeed a lower value of the cohesive strength has been selected in order to match the experimental results. This feature has been addressed with respect to the different interfacial stress profile produced by the trapezoidal model. From this standpoint, the extension of the process zone, which depends on the particular boundary value problem examined, could have an influence.

The present results do not allow one to conclude that CZMs with different shapes will always behave differently in fracture simulations. Whether or not this overestimation is of concern should be ascertained case by case and, above all, in the light of the scatter associated to the current experimental measurement methodologies. From this point of view proper experimental methodologies for determining the cohesive zone parameters are currently the subject of ongoing research.

## References

- ABAQUS user's manual (2002) v6.5-1. Pawtucket, USA, Hibbit, HKS Inc
- Akisanya AR, Fleck NA (1992) Brittle fracture of adhesive joints. *Int J Fract* 58(2):93–114. doi:[10.1007/BF00019971](https://doi.org/10.1007/BF00019971)
- Alfano G (2006a) On the influence of the shape of the interface law on the application of cohesive zone models. *Compos Sci Technol* 66(6):723–730. doi:[10.1016/j.compscitech.2004.12.024](https://doi.org/10.1016/j.compscitech.2004.12.024)
- Alfano M (2006b) Cohesive zone modeling of mode I fracture in adhesive joints. Technical Report, University of Illinois at Urbana Champaign, Illinois

- Alfano M, Furguele F, Leonardi L, Maletta C, Paulino GH (2007) Fracture analysis of adhesive joints using intrinsic cohesive zone model. *Key Eng Mater* 348:13–16
- ASTM D3433 (1999) Standard test method for fracture strength in cleavage of adhesives in bonded metal joints. American Society for Testing and Material, Philadelphia, PA, USA (Re-approved 2005)
- Barenblatt GI (1962) Mathematical theory of equilibrium cracks in brittle fracture. *Adv Appl Mech* 7:55–129
- Blackman B, Dear JP, Kinloch AJ et al (1991) The calculation of adhesive fracture energies from double-cantilever beam test specimens. *J Mater Sci Lett* 10(5):253–256. doi:[10.1007/BF00735649](https://doi.org/10.1007/BF00735649)
- Blackman B, Kinloch AJ, Paraschi M et al (2003a) Measuring the mode I adhesive fracture energy,  $G_{IC}$ , of structural adhesive joints: the results of an international round-robin. *Int J Adhes Adhes* 23(4):293–305. doi:[10.1016/S0143-7496\(03\)00047-2](https://doi.org/10.1016/S0143-7496(03)00047-2)
- Blackman B, Hadavinia H, Kinloch AJ et al (2003b) The calculation of adhesive fracture energies in mode I: revisiting the tapered double cantilever beam (TDCB) test. *Eng Fract Mech* 70(2):233–248. doi:[10.1016/S0013-7944\(02\)00031-0](https://doi.org/10.1016/S0013-7944(02)00031-0)
- Blackman B, Hadavinia H, Kinloch AJ et al (2003c) The use of a cohesive zone model to study the fracture of fibre composites and adhesively-bonded joints. *Int J Fract* 119(1):25–46. doi:[10.1023/A:1023998013255](https://doi.org/10.1023/A:1023998013255)
- Camacho GT, Ortiz M (1996) Computational modeling of impact damage in brittle materials. *Int J Solids Struct* 33(20–22):2899–2938. doi:[10.1016/0020-7683\(95\)00255-3](https://doi.org/10.1016/0020-7683(95)00255-3)
- Cox BN, Marshall DB (1991) The determination of crack bridging forces. *Int J Fract* 49(3):159–176
- Dugdale DS (1960) Yielding steel sheets containing slits. *J Mech Phys Solids* 8:100–104. doi:[10.1016/0022-5096\(60\)90013-2](https://doi.org/10.1016/0022-5096(60)90013-2)
- Ferracin T, Landis CM, Delannay F et al (2003) On the determination of the cohesive zone properties of an adhesive layer form the analysis of the wedge peel test. *Int J Solids Struct* 40(11):2889–2904. doi:[10.1016/S0020-7683\(03\)00076-3](https://doi.org/10.1016/S0020-7683(03)00076-3)
- Goglio L, Rossetto M (2002) Ultrasonic testing of anaerobic bonded joints. *Ultrasonics* 40(1–8):205–210
- Kafkalidis MS, Thouless MD, Yang QD, Ward SM (2000) Deformation and fracture of adhesive layers constrained by plastically-deforming adherends. *J Adhes Sci Technol* 14(13):1593–1607. doi:[10.1163/156856100742401](https://doi.org/10.1163/156856100742401)
- Kinloch AJ (1986) Adhesion and adhesives, science and technology. Chapman & Hall, London
- Liljedhal CDM, Crocombe AD, Wahab MA et al (2006) Damage modeling of adhesively bonded joints. *Int J Fract* 141(1–2):147–161. doi:[10.1007/s10704-006-0072-9](https://doi.org/10.1007/s10704-006-0072-9)
- Martiny P, Lani F, Kinloch AJ et al (2008) Numerical analysis of the energy contributions in peel tests: a steady-state multilevel finite element approach. *Int J Adhes Adhes* 28(4–5):222–236. doi:[10.1016/j.ijadhadh.2007.06.005](https://doi.org/10.1016/j.ijadhadh.2007.06.005)
- Mostovoy S, Ripling EJ (1971) Effect of joint geometry on the toughness of epoxy adhesives. *J Appl Polym Sci* 15(3):661–673. doi:[10.1002/app.1971.070150312](https://doi.org/10.1002/app.1971.070150312)
- Pardoen T, Ferracin T, Landis CM et al (2005) Constraint effect in adhesive joint fracture. *J Mech Phys Solids* 53(9):1951–1983. doi:[10.1016/j.jmps.2005.04.009](https://doi.org/10.1016/j.jmps.2005.04.009)
- Park K, Paulino GH, Roesler JR (2008) Determination of the kink point in the bilinear softening model for concrete. *Eng Fract Mech* 75(13):3806–3818. doi:[10.1016/j.engfracmech.2008.02.002](https://doi.org/10.1016/j.engfracmech.2008.02.002)
- Pirondi A, Nicoletto G (2000) Comportamento a frattura di un adesivo strutturale. Proceedings of the 15th National Congress of the Italian Group of Fracture, IGF XV, May 3rd–5th 2000, Bari, Italy, pp 459–466 (in Italian)
- Roesler JR, Paulino GH, Park K et al (2007a) Concrete fracture prediction using bilinear softening. *Cement Concr Compos* 29(4):300–312. doi:[10.1016/j.cemconcomp.2006.12.002](https://doi.org/10.1016/j.cemconcomp.2006.12.002)
- Roesler JR, Paulino GH, Gaedicke C et al (2007b) Fracture behavior of functionally graded concrete materials (FGCM) for rigid pavements. *Transp Res Rec* 2037:40–49. doi:[10.3141/2037-04](https://doi.org/10.3141/2037-04)
- Scheider I, Brocks W (2006) Cohesive elements for thin walled structures. *Comput Mater Sci* 37(1–2):101–109. doi:[10.1016/j.commatsci.2005.12.042](https://doi.org/10.1016/j.commatsci.2005.12.042)
- Shet C, Chandra N (2004) Effect of the shape of T- $\delta$  cohesive zones curves on the fracture response. *Mech Adv Mater Struct* 11(3):249–275. doi:[10.1080/15376490490427207](https://doi.org/10.1080/15376490490427207)
- Song SH, Paulino GH, Buttlar WG (2006a) Simulation of crack propagation in asphalt concrete using an intrinsic cohesive zone model. *J Eng Mech* 132(11):1215–1223. doi:[10.1061/\(ASCE\)0733-9399\(2006\)132:11\(1215\)](https://doi.org/10.1061/(ASCE)0733-9399(2006)132:11(1215))
- Song SH, Paulino GH, Buttlar WG (2006b) A bilinear cohesive zone model tailored for fracture of asphalt concrete considering viscoelastic bulk material. *Eng Fract Mech* 73(18):2829–2848. doi:[10.1016/j.engfracmech.2006.04.030](https://doi.org/10.1016/j.engfracmech.2006.04.030)
- Song SH, Paulino GH, Buttlar WG (2008) Influence of the cohesive zone model shape parameter on asphalt concrete fracture. In: *Multiscale and Functionally Graded Materials 2006*, edited by Paulino GH et al, 2008 American Institute of Physics Conference Proceedings, pp. 730–735
- Sorensen B, Jacobsen K (2003) Determination of cohesive laws by the J integral approach. *Eng Fract Mech* 70(14):1841–1858. doi:[10.1016/S0013-7944\(03\)00127-9](https://doi.org/10.1016/S0013-7944(03)00127-9)
- Tvergaard V, Hutchinson JW (1996) On the toughness of ductile adhesive joints. *J Mech Phys Solids* 44(5):789–800. doi:[10.1016/0022-5096\(96\)00011-7](https://doi.org/10.1016/0022-5096(96)00011-7)
- Volokh KY (2004) Comparison between cohesive zone models. *Commun Numer Methods Eng* 20(11):845–856. doi:[10.1002/cnm.717](https://doi.org/10.1002/cnm.717)
- Williams JG, Hadavinia H (2002) Analytical solutions for cohesive zone models. *J Mech Phys Solids* 50(4):809–825. doi:[10.1016/S0022-5096\(01\)00095-3](https://doi.org/10.1016/S0022-5096(01)00095-3)
- Xu X-P, Needleman A (1994) Numerical simulations of fast crack growth in brittle solids. *J Mech Phys Solids* 42(9):1397–1434. doi:[10.1016/0022-5096\(94\)90003-5](https://doi.org/10.1016/0022-5096(94)90003-5)
- Xu C, Siegmund T, Ramani K (2003) Rate dependent crack growth in adhesives I. Modelling approach. *Int J Adhes Adhes* 23(1):9–13. doi:[10.1016/S0143-7496\(02\)00062-3](https://doi.org/10.1016/S0143-7496(02)00062-3)
- Yang QD, Thouless MD, Ward SM (1999) Numerical simulations of adhesively bonded beams failing with extensive plastic deformation. *J Mech Phys Solids* 47(6):1337–1353. doi:[10.1016/S0022-5096\(98\)00101-X](https://doi.org/10.1016/S0022-5096(98)00101-X)
- Yuan H, Xu Y (2008) Computational fracture mechanics assessment of adhesive joints. *Comput Mater Sci* 43(1):146–156. doi:[10.1016/j.commatsci.2007.07.053](https://doi.org/10.1016/j.commatsci.2007.07.053)

- Zavattieri PD, Espinosa HD (2001) Grain level analysis of crack initiation and propagation in brittle materials. *Acta Mater* 49(20):4291–4311. doi:[10.1016/S1359-6454\(01\)00292-0](https://doi.org/10.1016/S1359-6454(01)00292-0)
- Zhang Z (2007) Extrinsic cohesive modeling of dynamic fracture and microbranching instability using a topological data structure. PhD Dissertation, University of Illinois at Urbana-Champaign
- Zhang Z, Paulino GH (2005) Cohesive zone modeling of dynamic failure in homogeneous and functionally graded materials. *Int J Plast* 21(16):1195–1254. doi:[10.1016/j.ijplas.2004.06.009](https://doi.org/10.1016/j.ijplas.2004.06.009)